# Measurement of the mean centraloptical depth of galaxy clusters via the pairwise kinematic Sunyaev-Zel'dovich effect with SPT-3G and DES

E. Schiappuco, <sup>1</sup> F. Bianchinio, <sup>2,3,4</sup> M. Aguena, <sup>5</sup> M. Archipleyo, <sup>6,7</sup> L. Balkenholo, <sup>1</sup> L. E. Bleema, <sup>8,9</sup> P. Chaubal, <sup>1</sup> T. M. Crawford, <sup>9,10</sup> S. Grandis, <sup>11,12</sup> Y. Omori, <sup>13,3,14,15</sup> C. L. Reichardt, <sup>1</sup> E. Rozo, <sup>1</sup> E. S. Rykoffo, <sup>14,17</sup> C. To, <sup>18</sup> T. M. C. Abbott, <sup>19</sup> P. A. R. Ade, <sup>2</sup> O. Alves, <sup>21,22</sup> A. J. Anderson, <sup>23,9,10</sup> F. Andrade-Oliveira, <sup>1</sup> J. Anniso, <sup>24</sup> J. S. Avva, <sup>2</sup> D. Bacon, <sup>26</sup> K. Benabed, <sup>27</sup> A. N. Benden, <sup>8,9</sup> B. A. Benson, <sup>23,9,10</sup> G. M. Bernsteir, <sup>28</sup> E. Bertin, <sup>29,30</sup> S. Bocquet, <sup>31</sup> F. R. Bouchet, <sup>27</sup> D. Brooks, <sup>32</sup> D. L. Burke, <sup>15,17</sup> J. E. Carlstrom, <sup>33,34,8,10</sup> A. Carnero Roself, <sup>52,36</sup> M. Carrasco Kind, <sup>7,6</sup> J. Carretero, <sup>38</sup> T. W. Cecib, <sup>8</sup> C. L. Chang, <sup>8,9,10</sup> P. M. Chichura, <sup>34,9</sup> T.-L. Chou, <sup>34,9</sup> M. Costanz, <sup>9,40,41</sup> A. Cukiermar, <sup>24,3</sup> L. N. da Costa, <sup>2</sup> C. Daleyo, <sup>6</sup> T. de Haan, <sup>42</sup> S. Desain, <sup>43</sup> K. R. Dibert, <sup>10,9</sup> H. T. Diehlo, <sup>24</sup> M. A. Dobbs, <sup>44,45</sup> P. Doel, <sup>32</sup> C. Doux, <sup>34,9</sup> D. Dutchen, <sup>34,9</sup> S. Everett, <sup>64</sup> W. Everett, <sup>47</sup> C. Feng, <sup>48</sup> K. R. Ferguson, <sup>49</sup> I. Ferrero, <sup>50</sup> A. Fert, <sup>46</sup> B. Flaugheo, <sup>24</sup> A. Foster, <sup>51</sup> J. Frieman, <sup>24,14</sup> S. Galli, <sup>27</sup> A. E. Gambre, J. García-Bellido, R. W. Gardner, M. Gatti, <sup>28</sup> T. Giannantonio, <sup>53,54</sup> N. Goeckner-Wald, <sup>2</sup> D. Gruen, <sup>31</sup> R. Gualtierio, <sup>8</sup> S. Guns, <sup>25</sup> G. Gutierrez, <sup>24</sup> N. W. Halverson, <sup>47,55</sup> S. R. Hinton, <sup>56</sup> E. Hivon, <sup>27</sup> G. P. Holdero, <sup>57</sup> D. L. Hollowood, <sup>58</sup> W. L. Holzapfel, <sup>58</sup> K. Honscheid, <sup>18,59</sup> J. C. Hood, N. Huang, <sup>25</sup> D. J. James, <sup>60</sup> L. Knox, <sup>61</sup> M. Korman, <sup>51</sup> K. Kuehn, <sup>62,63</sup> C.-L. Kuo, <sup>2,34</sup> Q. Lahavo, <sup>32</sup> A. T. Lee, <sup>25,64</sup> C. Lidman, <sup>65,66</sup> M. Lima, <sup>67,22</sup> A. E. Lowitz, <sup>9</sup> C. Lu, <sup>57</sup> M. March, <sup>28</sup> J. Mena-Fernández, <sup>68</sup> F. Menantean, <sup>37,6</sup> M. Millea, <sup>25</sup> R. Miquelo, <sup>69,38</sup> J. J. Mohr, <sup>34,9</sup> A. Rahlino, <sup>23,9</sup> M. Raveri, <sup>8</sup> M. Rodriguez-Monroy, <sup>7</sup> A. A. Plazas Malagón, K. Prabhu, J. Prat, <sup>31,14</sup> W. Quan, <sup>34,9</sup> A. Rahlino, <sup>23,9</sup> M. Raveri, <sup>8</sup> M. Rodriguez-Monroy, <sup>7</sup> A. R. Coorne, <sup>70</sup> M. Rouble, <sup>44</sup> J. E. R

#### (SPT-3G and DES Collaborations)

```
<sup>1</sup>Schoolof Physics,University ofMelbourne,Parkville, Victoria 3010, Australia
           <sup>2</sup>Kavli Institute for Particle Astrophysics and Cosmologytanford University,
                         452 Lomita Mall, Stanford, California, 94305, USA
<sup>3</sup>Department ofPhysics,Stanford University,382 Via Pueblo Mall,Stanford,California, 94305,USA
<sup>4</sup>SLAC NationalAccelerator Laboratory2575 Sand HillRoad,Menlo Park,California, 94025,USA
                       <sup>5</sup>Laboratório Interinstitucionalde e-Astronomia-LIneA,
                 Rua Gal. José Cristino 77, Rio de Janeiro, RJâ 20921-400 Prazil
                <sup>6</sup>Departmentof Astronomy,University of Illinois Urbana-Champaign,
                       1002 WestGreen StreetUrbana, Illinois, 61801, USA
       <sup>7</sup>Center for AstroPhysicaSurveys,National Center for Supercomputing Applications,
                                    Urbana, Illinois, 61801, USA
                   <sup>8</sup>High-Energy Physics DivisionArgonne NationalLaboratory,
                      9700 South Cass Avenue emont, Illinois, 60439, USA
                  <sup>9</sup>Kavli Institute for CosmologicaPhysics,University of Chicago,
                      5640 South Ellis Avenu@hicago, Illinois, 60637, USA
                <sup>10</sup>Departmentof Astronomy and AstrophysickIniversity of Chicago,
                      5640 South Ellis Avenu@hicago, Illinois, 60637, USA
           <sup>11</sup>University ObservatoryFaculty of Physics,Ludwig-Maximilians-Universität,
                               Scheinerstr.1, 81679 Munich, Germany
            <sup>12</sup>Excellence Cluster ORIGINSSoltzmannstr2, 85748, Garching, Germany
 <sup>13</sup>Department ofAstronomy and AstrophysicЫniversity ofChicago,Chicago,Illinois 60637,USA
   <sup>14</sup>Kavli Institute for Cosmological PhysicsJniversity ofChicago,Chicago,Illinois 60637,USA
   <sup>15</sup>Kavli Institute for Particle Astrophysics & Cosmolog P. O. Box 2450, Stanford University,
                                  Stanford, California 94305, USA
            <sup>16</sup>Department of Physics, University of Arizona, Tucson, Arizona 85721, USA
           <sup>17</sup>SLAC NationalAccelerator LaboratoryMenlo Park, California 94025, USA
           <sup>18</sup>Center for Cosmology and Astro-Particle Physic Physic Ohio State University,
                                    Columbus, Ohio 43210, USA
```

```
<sup>19</sup>Cerro Tololo Inter-American ObservatorNSF's NationalOptical-Infrared Astronomy
                         Research LaboratoryCasilla 603, La Serena,Chile
     <sup>20</sup>Schoolof Physics and AstronomyCardiff University, Cardiff CF24 3YB, United Kingdom
         <sup>21</sup>Department of Physics University of Michigan, Ann Arbor, Michigan 48109.USA
                       <sup>22</sup>Laboratório Interinstitucionalde e-Astronomia—LIneA,
                  Rua Gal. José Cristino 77, Rio de Janeiro, RJ 20921-400 Brazil
   <sup>23</sup>Fermi National Accelerator LaboratoryMS209,P.O. Box 500,Batavia,Illinois, 60510,USA
        <sup>24</sup>Fermi National Accelerator Laboratory P. O. Box 500, Batavia, Illinois 60510, USA
         <sup>25</sup>Department of Physics, University of California, Berkeley, California, 94720, USA
   <sup>26</sup>Institute of Cosmology and Gravitation University of Portsmouth, PO1 3FX United Kingdom
             Institut d'Astrophysique de ParisUMR 7095, CNRS & Sorbonne Universet
                            98 bis boulevard Arago,75014 Paris, France
 <sup>28</sup>Department of Physics and Astronomy University of Pennsylvania Philadelphia, PA 19104, USA
            <sup>9</sup>CNRS,UMR 7095, Institut d'Astrophysique de ParisF-75014, Paris, France
                      <sup>30</sup>Sorbonne Universets, UPMC Univ Paris 06, UMR 7095,
                      Institut d'Astrophysique de Paris F-75014, Paris, France
            <sup>31</sup>University ObservatoryFaculty of Physics,Ludwig-Maximilians-Universität,
                               Scheinerstr.1, 81679 Munich, Germany
                  <sup>32</sup>Department of Physics & Astronomy University College London,
                         Gower Street London, WC1E 6BT, United Kingdom
<sup>33</sup>Enrico Fermi Institute, University of Chicago, 5640 South Ellis Avenue, Chicago, Illinois, 60637, USA
<sup>34</sup>Department of Physics, University of Chicago, 5640 South Ellis Avenue, Chicago, Illinois, 60637, USA
              35Instituto de Astrofisica de Canaria -38205 La Laguna, Tenerife, Spain
        <sup>36</sup>Universidad de La LagunaDpto. AstrofÃsica,E-38206 La Laguna,Tenerife,Spain
        <sup>37</sup>Center for AstrophysicaSurveys, National Center for Supercomputing Applications,
                          1205 WestClark St., Urbana, Illinois, 61801, USA
   <sup>38</sup>Institut de Física d'Altes Energies (IFAE)The Barcelona Institute o$cience and Technology,
                          Campus UAB 08193 Bellaterra (Barcelona) Spain
<sup>39</sup>Astronomy Unit,Department ofPhysics,University of Trieste, via Tiepolo 11,I-34131 Trieste,Italy
       <sup>40</sup>INAF-Osservatorio Astronomico d∎rieste,via G. B. Tiepolo 11,I-34143 Trieste,Italy
        <sup>41</sup>Institute for FundamentaPhysics of the Universe, Via Beirut 2, 34014 Trieste Italy
    <sup>42</sup>High Energy Accelerator Research Organization (KEK)sukuba baraki 305-0801, Japan
               <sup>3</sup>Departmentof Physics,IIT Hyderabad,Kandi, Telangana 502285India
               <sup>44</sup>Departmentof Physics and McGillSpace InstituteMcGill University,
                      3600 Rue UniversityMontreal, Quebec H3A 2T8Canada
 <sup>45</sup>Canadian Institute for Advanced Resear@IFAR Program in Gravity and the Extreme Universe,
                                 Toronto, Ontario, M5G 1Z8, Canada
                   <sup>46</sup>Jet Propulsion Laboratory,California Institute of Technology,
                       4800 Oak Grove Dr., Pasadena California 91109, USA
        <sup>47</sup>CASA, Department of Astrophysical Planetary Science Iniversity of Colorado,
                                   Boulder, Colorado, 80309, USA
<sup>48</sup>Department of Astronomy, School of Physical Sciences, University of Science and Technology of China,
                                     Hefei, Anhui 230026, China
<sup>49</sup>Department of Physics and Astronomy, University of California, Los Angeles, California, 90095, USA
                      <sup>50</sup>Institute ofTheoreticalAstrophysicsUniversity ofOslo.
                           P.O. Box 1029 Blindern, NO-0315 Oslo, Norway
      <sup>51</sup>Departmentof Physics,Case Western Reserve Universit@leveland,Ohio, 44106,USA
  <sup>52</sup>Instituto de Fisica Teorica UAM/CSIQJniversidad Autonoma de Madriq28049 Madrid, Spain
                          <sup>53</sup>Institute of Astronomy, University of Cambridge,
                      Madingley Road Cambridge CB3 0HA United Kingdom
                      <sup>54</sup>Kavli Institute for CosmologyUniversity of Cambridge,
                      Madingley Road Cambridge CB3 0HAUnited Kingdom
          <sup>55</sup>Departmentof Physics, University of Colorado, Boulder, Colorado, 80309, USA
   <sup>56</sup>Schoolof Mathematics and Physics Iniversity of Queensland Brisbane, QLD 4072, Australia
                  <sup>57</sup>Departmentof Physics,University of Illinois Urbana-Champaign,
                        1110 WestGreen StreetUrbana, Illinois, 61801, USA
           <sup>58</sup>Santa Cruz Institute for Particle PhysicSanta Cruz, California 95064, USA
          <sup>59</sup>Departmentof Physics,The Ohio State UniversityColumbus,Ohio 43210,USA
         <sup>60</sup>Center for Astrophysics | Harvard & Smithsonia60 Garden StreetCambridge,
                                      Massachusetts 02138ISA
```

<sup>61</sup>Department of Physics & Astronomy University of California, One Shields Avenu@avis, California 95616, USA <sup>62</sup>Australian Astronomical Optics, Macquarie University, North Ryde, New South Wales 2113, Australia 63Lowell Observatory,1400 Mars Hill Rd, Flagstaff, Arizona 86001,USA <sup>64</sup>Physics DivisionLawrence Berkeley National Aboratory, Berkeley, California, 94720, USA <sup>65</sup>Centre for Gravitational Astrophysic College of Science, The Australian National University, ACT 2601, Australia <sup>66</sup>The Research Scho**o**lf Astronomy and Astrophysics, Australian National University, ACT 2601, Australia <sup>67</sup>Departamento de Física Matemáticanstituto de Física, Universidade de São Paulo, CP 66318, São Paulo, São Paulo, 05314-970, Brazil <sup>68</sup>Centro de Investigaciones En**œtj**ćas,Medioambientales y Tecnológicas (CIEMA**™**)adrid, Spain <sup>69</sup>Institució Catalana de Recerca i Estudis Avança**E**s,08010 BarcelonaSpain <sup>70</sup>Max Planck Institute for ExtraterrestriaPhysics, Giessenbachstrass **8**5748 Garching, Germany <sup>71</sup>Perimeter Institute for Theoretical Physics, 31 Caroline St. North, Waterloo, Ontario N2L 2Y5, Canada <sup>72</sup>Materials Sciences DivisionArgonne NationalLaboratory. 9700 South Cass Avenueemont, Illinois, 60439, USA <sup>73</sup>Observatório NacionalRua Gal. José Cristino 77, Rio de Janeiro, RJ 20921-400 Brazil <sup>74</sup>California Institute of Technology, 1200 East California Boulevard., Pasadena, California, 91125, USA <sup>5</sup>Hamburger SternwarteUniversitätHamburg,Gojenbergsweg 11221029 Hamburg,Germany <sup>76</sup>Departmentof AstrophysicalSciencesPrinceton University, Peyton Hall, Princeton, New Jersey 08544USA <sup>77</sup>Department of Physics and Astronomy Pevensey Building, University of SussexBrighton, BN1 9QH, United Kingdom <sup>78</sup>Three-Speed Logidnc., Victoria, B.C., V8S 3Z5, Canada <sup>79</sup>School of Physics and Astronomy, University of Southampton, Southampton, SO17 1BJ, United Kingdom <sup>80</sup>Computer Science and Mathematics Divisi**®a**k Ridge NationaLaboratory, Oak Ridge, Tennessee 3783 USA

<sup>81</sup>Lawrence Berkeley Nationalaboratory, 1 Cyclotron Road, Berkeley, California 94720, USA 82 Universitäts-Sternwarte, akultät für Physik, Ludwig-Maximilians Universitä München,

Scheinerstr.1, 81679 MünchenGermany

<sup>83</sup>Department of Physics and Astronomy, Michigan State University, East Lansing, Michigan 48824, USA

(Received 26 July 2022accepted 12 December 2022ublished 21 February 2023)

We infer the mean optical depth of a sample of optically selected galaxy clusters from the Dark Energy Survey via the pairwise kinematic Sunyaev-Zel'dovich (KSZ) effette pairwise KSZ signal between pairs of clusters drawn from the Dark Energy Survey Year-3 cluster catalog is detected at 4.1σ in cosmic microwave background temperature maps from two years of observations with the SPT-3G camera on the South Pole Telescope. After cuts, there are 24,580 clusters in the ~1? 400hdexputhern sky observed by both experimentsWe infer the mean opticadepth of the cluster sample with two technique the optical depth inferred from the pairwise KSZ signal is  $\overline{0}2.97 \quad 0.73$   $\times 10^{3}$ , while that inferred from the thermal SZ signal is  $\bar{\tau}_e \frac{1}{4}$   $\delta 2.51 \ 0.55^{\text{stat}} \ 0.15 \ ^{\text{syst}} > 10^3$ . The two measures agree  $\delta 0.6\sigma$ . We perform a suite of systematic checks to tebe robustness of the analysis.

DOI: 10.1103/PhysRevD.107.042004

#### I. INTRODUCTION

The Sunyaev-Zel'dovich (SZ) effect1,2] occurs when free electrons in the hot intracluster medium of galaxy clusters inverse Compton scattephotons of the cosmic microwave background (CMB). The SZ effect is one of the ffect has been measured through its contribution to the powerful probes of astrophysics and cosmology (e.g., [3,4]). The SZ effect is normally subdivided into the thermal and kinematic Sunvaev-Zel'dovich effects.The thermal SZ (TSZ) effect is due to an energy transfer from [11]. However, measuring the KSZ effect is of great interest

the hot electrons to the CMB photons, distorting the CMB black body spectrum by shifting photons to higher frequencies. The kinematic SZ (KSZ) effect is due to the bulk velocity of the electrons slightly changing the apparent temperature of the black body spectrum. While the TSZ largest sources of secondary CMB anisotropy and enable MB power spectrum and bispectrum, and detected at the individual cluster level [5-10], measuring the KSZ effect is more challenging becauseof its lower amplitude and spectral degeneracy with the CMB temperature fluctuations since it could potentially be used to constrain both cosmological and astrophysica barameters [12-15] particularly breaking the f –  $\sigma_8$  degeneracy that ther cosmological probes are incapable of resolving [16].

Although the amplitude of the KSZ signal is small,

recent studies have detected the effect. The first detection afasets. In Sec. VI, we present our results, compare with the KSZ signal was made using high-resolution CMB datasimulations, discuss some robustnesstests as well as from the Atacama Cosmology Telescope [17] in conjunc-systematics thatould affect the observed signaland the release 9 spectroscopic galaxy catalog [18]A pairwise statistical approach was applied to measure the KSZ signal, Sec. VII and discuss the main implications for future which takes into account that on average clusters are falliagalyses. towards each other due to gravity and this gives rise to a signal that can be measured. This technique led to a rejection of the null-signal hypothesis with a p-value of 0.002 [19]. This pairwise approach was also adopted in a translate redshifts into distances: 1/H67.66 kms<sup>-1</sup> Mpc<sup>-1</sup> similar analysis using data from the SPT-SZ camera on the h21/40.11933, Qh21/40.02242, g1/40.8102, g1/40.9665. South Pole Telescope [20,21] and the Dark Energy Survey (DES) [22] Year 1 cluster catalog [23], which resulted in a

Digital Sky Survey galaxy catalog [24], and Planck collaboration CMB data in conjunction with the Dark Energy Spectroscopic Instrumehegacy Imaging survey galaxy catalog [25], reported >  $5\sigma$  evidence for the pairwise KSZ signal. These analyses used spectroscopic galaxy

4.2σ detection of the pairwise signal. This was the first

catalogs which provide more accurate redshiftneasurements in comparison with photometric catalogs, a key feature for detecting the pairwise KSZ signal at high significance. Other methods such as the projected fields was used to measure the KSZ signalvith a 6.5σ detection [27].

In this work, we use the CMB temperature maps from SPT-3G, the third-generation camera on the SPT and a cluster catalog from Year 3 DES data (DES-Y3) to probe there of galaxy clusters to fall towards one anotheron filter to extract the clusters' SZ imprints on temperatures KSZ effect, two clusters falling towards one another will from the CMB maps and then applying a pairwise statistical ave a potentially detectable dipole pattern on the CMB approach to the catalog. We also test the robustness of themperature anisotropy (e.g[33]). This pattern is called measurement by using different covariance estimation teqhe pairwise KSZ (PKSZ) signal. The average PKSZ niques, null tests, and an analysis of systematics. As a finamplitude T<sub>PKSZ</sub>ðrÞ for all the pairs of galaxy clusters at a  $y - \tau$  scaling relation calibrated on N-body simulations velocity  $v_{12}$  of the clusters:

[28], similarly to previous work [29,30]. Measuring the TSZ simultaneously with KSZ can break the degeneracy with astrophysics of the KSZ effect and thus be very usefulo constrain cosmology.

The paper is organized as follows. In Sec. II, we briefly the halo pairwise velocity, and the theoretical template used attentions on scales of 8 Mpc, and the spectral index for modeling the expected signal. The DES and SPT

datasets used in this analysis are introduced in Setll. In Sec. IV, we detail the analysis methods that use to recover the signal from the data, before describing in Sec. V the set of simulations that we use to verify our pipeline and to estimate the detection significance expected for our

tion with the Baryon Oscillation Spectroscopic Survey datastimation of the mean optical depth of the cluster catalog through the TSZ. Finally, we briefly summarize our results

> We use the ΛCDM model with the best-fit Planck 2018 [31] TT b TE b EE b lowE b lensing b BAO cosmological parameters to compute theoretical redictions and to

#### II. THEORETICAL BACKGROUND

study to probe the KSZ signal using a photometric redshiftA. The pairwise kinematic Sunyaev-Zel'dovich effect cluster sample. More recent analyses using newer AtacamaThe KSZ effect from a galaxy cluster i producesa Cosmology Telescope CMB data combined with the Sloan fractional shift in the CMB temperature  $\Delta T_{\overline{c}MB}$  proportional to the cluster's velocity, valong the line of sight;

$$\frac{\Delta T}{T_{CMB}} \tilde{\delta f}_i \triangleright \frac{1}{4} - \xi_{;i} \frac{\hat{f}_i \cdot v_i}{c}; \qquad \qquad \tilde{0}1 \triangleright$$

where c is the speed of light and is the Thomson optical depth for CMB photons traversing the cluster[2]. This expression assumes a single scattering per photon, which is a good assumption at the low optical depth<sub>i</sub>(≴ 0.01) of [26] technique have obtained a 3.8–4.2σ detection of the most galaxy clusters. A unique property that the KSZ effect KSZ effect, meanwhile a velocity reconstruction approach over the generally brighter TSZ effect is that the KSZ effect depends on the bulk momentum of the ionized cluster gas along the line of sight, and thus can enable tests of the cosmological velocity field [32].

On scales smaller than the homogeneity scale, we expect pairwise KSZ effect. We achieve this by applying a matchederage due to their mutual gravitational pull. Through the test, we derive the mean optical depth from the TSZ by using oving separation r can be related to the mean pairwise

$$T_{PKSZ} \tilde{o} r P \equiv T_e \frac{v_{12} \tilde{o} r P}{c} T_{CMB};$$
  $\tilde{o} 2 P$ 

<sup>1</sup>The cosmological parameters listed are the Hubble parameter, describe the theory behind the KSZ effect, its connection to cold dark matter density, baryon density, current rms of the linear of the primordial scalar fluctuations espectively.

where ten is the average optical depth of the samplehis equation is valid with two assumptions: (i) the internal motion of the cluster does not introduce any sout bias, and (ii) there is no strong correlation between the optical depth and the velocity of the individual clusters [34]We adopt a sign convention so that clusters falling towards or teigh-passfilter set at  $k_x > 500$ . The filtered TOD are another will have a negative relative velocity 15 or and negative  $T_{KSZ}$  signal.

We can predict the relative velocity as a function of distance, v<sub>12</sub> or Þ, for a specific cosmology and theory of gravity from the statistical distribution of the dark matter haloes. The mean pairwise velocity of haloes v<sub>12</sub>ðrÞ separated by their comoving distance r 1/4 jc2 - rat can be analytically modeled in linear theory in terms of the twdemperature maps, respectively. At each frequency, the point matter correlation function ξorb as (e. (g3,5-37])

$$v_{12}$$
ðr;  $ab \approx \frac{2}{3}aH$ ðaÞfðaÞ $\frac{b\xi$ ðrÞ}{1 b b²ξðrÞ}; ð3Þ

where a is the scale factor, Hoap the Hubble parameter,  $f\eth a \triangleright \equiv d \ln D = d \ln a$  is the growth rate (with D being the linear growth factor), b the mass-averaged halo bias and indicates the average of ξõrÞ over a comoving sphere of optically selected galaxy clusters from the firstthree radius r.

PKSZ are sensitive to a combination of both cluster astrophysicsthrough the optical depth Te and halo bias b, and cosmology through the Hubble parameter Hoab, the bservatory in northern Chile. The cluster catalog has growth rate f, and the two-point matter correlation function been extracted from DES Year-3 observations with the  $\xi \delta r P$ . In particular, the dependence on the growth rate f and redMaPPer algorithm [44]. the matter correlation function ξỗrÞ makes measurements of the redMaPPeralgorithm is a red-sequence the PKSZ signal consitive to fα<sup>2</sup>. This provides complements of the PKSZ signal consitive to fα<sup>2</sup>. This provides complements of the PKSZ signal consitive to fα<sup>2</sup>. This provides complements of the PKSZ signal consitive to fα<sup>2</sup>. This provides complements of the provides complements of the redMaPPeralgorithm is a red-sequence as the PKSZ signal consistive to fα<sup>2</sup>. This provides complements of the redMaPPeralgorithm is a red-sequence as the provides complements of the redMaPPeralgorithm is a red-sequence as the provides complements of the redMaPPeralgorithm is a red-sequence as the provides complements of the redMaPPeralgorithm is a red-sequence as the provides complements of the redMaPPeralgorithm is a red-sequence as the provides complements of the provides complements of the redMaPPeralgorithm is a red-sequence as the provides complements of the provides complement the PKSZ signalsensitive to fo<sub>8</sub><sup>2</sup>. This provides compledistortions, which are primarily sensitive to (e.g., [16]), and hence could be used to probe dark energy and modifications of gravity (e.g.,[37–39]).

#### III. DATA

# A. SPT-3G temperature maps

3G, the third and latest camera installed on the South Polene quenching of star formation due to the cluster's located at the Amundsen-ScottSouth Pole Station in Antarctica. The SPT-3G focalplane consists of ~16; 000 multichroic, polarization-sensitiveransition-edgesensor bolometers which operate in three bands 95, 150, and 220 GHz, with an angular resolution of 40]. The main SPT-3G survey field of approximately 1; 500 dextends from -42° to -70° in declination and -50° to 50° in right ascension. This work uses temperature maps from observenth and complete above a certain luminosity/hile the 2019 and 2020.

We refer to [41] for a full description of how the timeordered data (TOD) are converted into madaut we will provide a succinct description of the procedures below. The TOD for each of the SPT-3G bolometers are filtered to remove low-frequency noise in the scan directiowith a binned into map pixels with weights based on the TOD noise level, and calibrated such thathe map is in CMB fluctuation temperature units. A flat-sky approximation, the Sanson-Flamsteed projection [42,48], used for the map with 0.250 square pixels. The map noise levels measured in the 3000 < I < 5000 range are 5.0, 3.9, and 14.0 µK-arcmin for the coadded 95,150, and 220 GHz instrument beam is well represented with a Gaussian with full width at half maximum equal to 1.6 1.20, and 1.00 at 95, 150, and 220 GHz, respectively. Sections IV B and VI D describe how these multifrequency temperature maps are used to extract the CMB b KSZ or Compton-y maps.

#### B. DES Year-3 redMaPPer cluster catalog

The second data product used in this analysis is a sample years of the DES.DES is a photometric survey thathas Equations (2) and (3) highlight that measurements of the appeal out ~5000 degof the southern sky in the optical to near-infrared bands using the Dark Energy Camera [22], mounted on the 4-meter Blanco telescope at Cerro Tololo

mentary information to other probes such as redshift space able. The outputs from redMaPPer relevant to the present analysis are as follows: (i) the cluster's sky position, given by the angular coordinates of the algorithm's best guess for the central galaxy position; (ii) the cluster's photometrically estimated redshift(iii) the optical richness estimate λa weighted sum of the membership probabilities, which is a low-scatter proxy for the cluster mass (e. \$45,461). The underlying idea is that galaxy clusters are concentrations of In this analysis, we use CMB temperature maps from Spalaxies containing old red stars thought to be caused by Telescope (SPT) [20,21]. The SPT is a 10-meter telescopenvironment. Therefore, the algorithm detects candidates by identifying over-densities of luminous red galaxies and iteratively assigns membership and probabilities for each

galaxy identified to be part of a cluster candidate to be in the center of the cluster. The redMaPPer algorithm has been used to produce both

a flux-limited and volume-limited sample using DES Y3 data. The volume-limited sample is independent of survey tions made during the winter season (March-September) this-limited sample contains more high-z clusters detected in the deeper fields in the survey. In this work, we use the

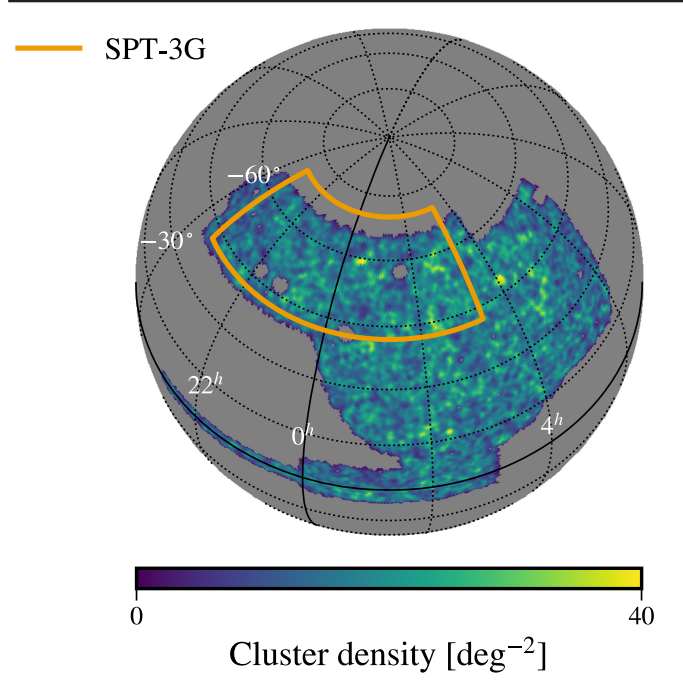


FIG. 1. Number density of the DES Y3 clusters with 1060, smoothed with a Gaussian kernel with \$4 1 deg for visualization purposes. The solid orange line shows the boundaries density of 17.6 clusters=defor our  $10 \le \tilde{\lambda} \le 60$  baseline SPT-3G main survey footprin These two datasets overlap over sample, with a mean redshift of  $\bar{z} \, \% \, 0.54 \, \delta 0.52 \, kand \, a$ approximately 1;400 deg

flux-limited catalog. This catalog contains 41,219 (8,712) clusters in the richness rangeλ > 10ð20Þ and spans the photo-z range 0.1 < z < 0.95.

We restrict the baseline cluster sample used in this work to  $z \le 0.8$  to mitigate the degradation at high redshifts of the completeness and photo-z accuracy. We also impose a mplement the PKSZ estimator  $\hat{T}_{PKSZ}$  introduced by cutoff at  $\tilde{\lambda} \le 60$  to eliminate the most massive clusters due [48]. This estimator for the mean PKSZ signal is to concerns about the possibility that the filtering described in Sec. IV B will not completely remove the contaminating signals from the cluster itself. We also considercluster samples with alternative richness ranges in Sec. VI to test the robustnessof the analysis and potential systematic biases.

~1; 400 deg, which we show in Fig. 1. We remove any clusters that are less than 1° from the survey edges, which ye the PKSZ signal) by a geometrical factor,  $c_{ij}$  ½ a conservative choice to enforce an homogeneous depth  $\ddot{\Gamma}_{ij}$  . coverage; or 10' distance from any point sources detecte  $\Phi$  eparation  $\hat{r}_{ij}$   $\frac{1}{4}$   $\hat{r}_i$  -  $\hat{r}_j$  onto the line of sight. in the SPT-3G map (≥ 6 mJy at 150 GHz) to avoid possible We reconstructhe pairwise KSZ signalin eight bins: contamination from the point sources onto the clusters. These cuts leave 24,580 (5,797); lusters in the richness range  $10\tilde{\delta}20$   $\neq \tilde{\lambda} < 60$ , which translates to a surface

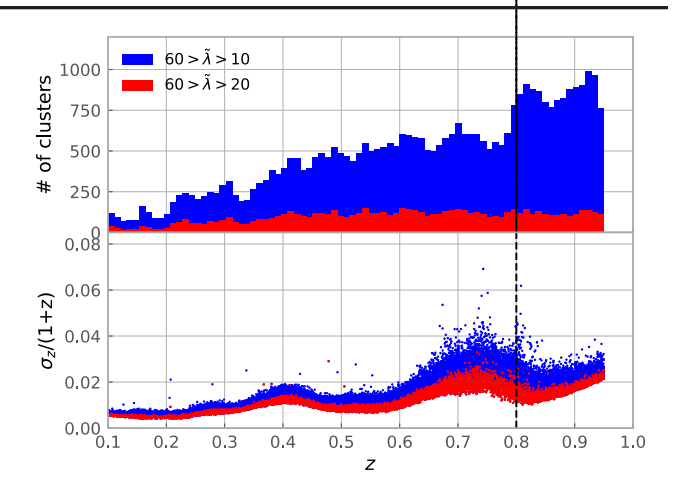


FIG. 2. Top: redshift distribution of the DES Y3 redMaPPer catalog for the two richness-based samples. Bottom: photometric redshift errors distribution for the DES Y3 redMaPPer clusters. In each panel, the red color denotes the 20 <  $\lambda$  < 60 sample whereas the blue color refers to our baseline \$\text{N} @ 60 sample. The vertical dashed black line represents the maximum redshift of clusters thatwe include in our analysis.

typical error in the photo-z of  $g \sim 0.01\delta1$  b zb [47].The redshift distribution and redshiftuncertainties of the full cluster sample are shown in Fig2.

## IV. ANALYSIS METHODOLOGY

# A. Pairwise KSZ estimator

As in previous measurements (e.g.19,23,24,29]),we

$$\begin{array}{c} P \\ \hat{T}_{PKSZ} \tilde{\delta} r \triangleright \frac{1}{4} - \frac{1}{2} \tilde{\delta}_{ij} \stackrel{\cdot}{\triangleright} - T \tilde{\delta}_{ij} \stackrel{\cdot}{\triangleright} c_{ij}}{\stackrel{\cdot}{\mapsto}_{i < j; r}}; \qquad \tilde{\delta} 4 \triangleright \end{array}$$

which scales the CMB temperature difference the two The DES and SPT-3G surveys overlap over a sky area cluster locations (which has an expectation value that depends on the relative velocity between the two clusters  $\hat{\sigma}_i \not = \hat{r}_i \not = 2$ ,to account for the projection of the pair

seven bins linearly separated between comoving pair separation r of 40 and 200 Mpc, plus a final bin that includes pairs separated by 200 to 300 Mpc. The choice of the minimum separation is motivated by the fathat the PKSZ template is derived within the linear regime, limiting the modeling of the pairwise velocities between halos correction factor based on local survey depth, masking, etc. This below r ≤ 40 Mpc (due to, e.g., nonlinearities and redshift space distortions) and because the photo-z errors significantly suppress the signal and increase the statistical

<sup>&</sup>lt;sup>2</sup>We apply cuts to the catalog using the raw galaxy counts that are related to the optical richness as  $\lambda \frac{1}{4} k$ , where s is a choice has been shown to yield a cluster sample with more uniform noise propertiessee [23] and references therein.

uncertainties. We choose to have a single bin at larger separations given that the PKSZ signal mostly arises frommaps at different observed frequencies. smaller and intermediate comoving separations so for scales larger than 200 Mpc the signal is significantly smaller.

#### B. CMB map filtering and temperature extraction

matched filter to the map, using prior knowledge of the spectral and angular dependence of the KSZ effect and other signals, to maximize the signal-to-noise ratio on the PKSZ signal. The filter Ψ for N<sub>v</sub> different observed frequencies v is constructed in Fourier space as

$$\Psi \delta v$$
;  $k \triangleright \frac{1}{4} \partial N^{-1} \delta v$ ;  $k \triangleright \cdot \mathcal{L} \delta v$ ;  $k \triangleright$ ;  $\delta 5 \triangleright$ 

where k is the Fourier mode, N<sup>-1</sup> ov; kÞ is the inverse of the noise covariance matrix of the map Sfilt ov; kp is the expected signal vector in Fourier space, and  $\sigma_{\Psi}^2$  is the predicted variance of the filtered map. In this work, we predicted variance of the filtered map. In this work, we  $\hat{T}_0 \hat{\sigma}_i \triangleright$ , as assume the cluster emission follows a projected isothermal  $\beta$  profile [49] with  $\beta$  ¼ 1, written in cluster-centric coordinates as

Tổ
$$\theta$$
Þ ¼ Tổ1 þ  $\theta$ = $\theta$ Þ¹; ð6Þ

taken as 91/4 0.59 throughout this work. The PKSZ results were found to be insensitive to the choice to higher noise levels [23], however we did not test this effect for the SPT 35 mooth temperature evolution. The choice of the second as mooth temperature evolution. data because the significance of detection of the PKSZ signal will not increase in a significant manner in comparison with [23] due to the intrinsic limit that come from photometric β profile, the instrumental beam, and map filtering.

We can estimate the variance of the filtered map from

We assume the noise is stationary, allowing the noise symmetrical  $N_v \times N_v$  matrix at each value of k, where the diagonal elements are the autopower spectra of every frequency map and the off-diagonal elements are the cross-spectra between the different frequencies.

The filter is built such that  $\hat{T}_0$ , an estimate of  $T_0$ , is extracted when centered on the cluster patisition  $\hat{\mathbf{n}}_0$  as

Z 
$$\hat{T}_0 \frac{1}{4} d^2 \hat{n} \Psi \delta v; \hat{n} - \hat{n}_0 \triangleright \cdot T \delta v, \hat{n} \triangleright; \delta 8 \triangleright$$

where Tov; np represents the vector of the temperature

We use three different matched filters in this work for different purposes. The first filter is a minimum variance multifrequency matched filter (MF-MF) with the 95150, and 220 GHz maps from SPT-3GThe second filter is a constrained minimum variance version (MF-TSZ), with the nonrelativistic TSZ effect nulled, following [50]. Third, The next step is to extract the CMB temperature shift dellowing [23], we build a single-frequency matched filter to the KSZ effect at the location of the clusters. We apply for the 150 GHz map (MF-150 GHz); the 150 GHz map has the lowest noise level of the three frequency bandsat 3.9 µK-arcmin.

# C. Redshift-dependent foregrounds

Over an extended redshift range, the redshift evolution of TSZ signal and cosmic infrared background (CIB) emission can potentially introduce a redshift-dependent bias in the estimated temperatures. To mitigate any such redshiftdependent effects, we estimate the mean measured temperature as a function of redshift and subtract this mean temperature from the matched-filtered temperature values

$$\begin{array}{c}
P \\
\hat{J}_0 \tilde{m}_j \triangleright G \tilde{g}_z ; \Sigma_z \triangleright \\
\tilde{G} \tilde{g}_z; \Sigma_z \triangleright
\end{array}$$

$$\begin{array}{c}
P \\
\tilde{J}_0 \tilde{m}_j \triangleright G \tilde{g}_z ; \Sigma_z \triangleright \\
\tilde{G} \tilde{g}_z; \Sigma_z \triangleright
\end{array}$$

$$\begin{array}{c}
\tilde{g}_2 \tilde{g}_3 \tilde{g}_3 = \tilde{g}_3 =$$

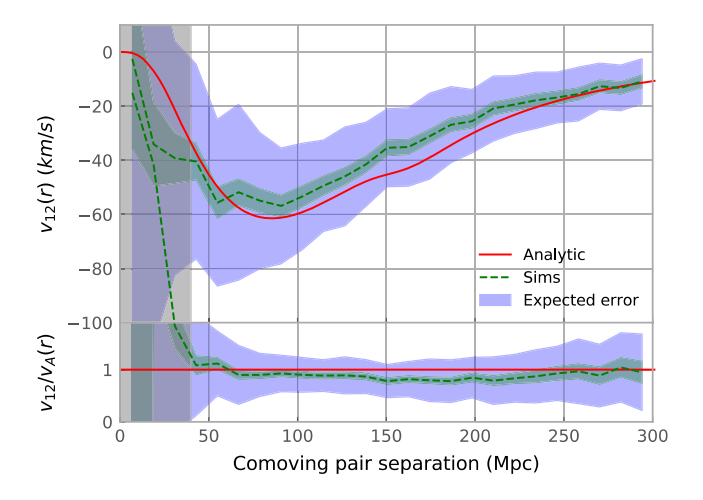
The smoothed temperature atzi is calculated from the weighted sum of contributions of clusters at redshift zi with  $\theta_c$  being the angular core radius of the cluster, which is ing a Gaussian kernelGðz;  $z_j$ ;  $z_z$   $z_j$   $z_j$ ỗ2♀Þ. For this analysis, we choose ₹ 0.02 resulting in

#### D. Analytical modeling of the photo-z uncertainties

redshift uncertainties, as shown in Sec. V B. The expected Redshift uncertainties are the dominant source of error in signal template in the matched filter is the convolution of this calculation of the separation distance between cluster pairs. The redshift errors, leads to a rms uncertainty in the comoving distances,  $d_{Q}^{2}$   $d_{Q}^{2}$  coz=HðzÞ [23]. For the sample used in this work we find  $\sigma_{d_c} \approx 80$  Mpc. Redshifterrors completely dilute the signal at  $r \ll \sigma_{d_c}$ , the signal is significantly reduced on scales r a, pand the signal from cluster pairs with  $r \gg \sigma_{d_c}$  is unaffected. Following the prescription from [23], we account for the smoothing due covariance matrix of the maps Nov; kp to be expressed as the uncertain distances by multiplying the pairwise KSZ template in Eq. (2) by an exponential term to suppress the signal at small scales:

$$T_{PKSZ}$$
ðr; ab  $\frac{v_{12}}{c}T_{CMB} \times 1 - exp - \frac{r^2}{2\sigma_r^2}$  : ð10b

As in [23], we take the smoothing scale to be  $5\sigma^{0}$  p fiffiffiffing  $2\sigma_{d_{c}}$ . We test the analytic approach with simulations and find good agreement as shown in Fig. 3.



52 75 0.8 Comoving distance (MPc) 97 0,6 120 143 0.4 165 0.2 188 250 0.0 120 143 165 188 Comoving distance (MPc)

FIG. 3. A comparison between the analytical model (solid red FIG. 4. Correlation matrix of the PKSZ measurement shown in Fig. 6 calculated with 1,000 jackknife subsample The higher line) of the mean pairwise velocity  $v_{12}$  or P compared to one obtained through simulations described in Sec. VA (dashed gredistance bins show more correlation because on average we line), corrected with Eq. (10) to account for the Gaussian photoexcounter the same clusters more times. errors of the clusters of  $\sigma$  0.01, similar to the one measured for the DES cluster catalogThe wider shaded blue area shows the expected errorbars from the PKSZ reconstruction for years of SPT-3G temperature mapsThe simulated cluster sample contains N 1/4 22; 923 clusters within a mass range of 0.6 <  $M_{500c}$ =10<sup>14</sup> $M_{\odot}$  < 4 between redshifts of 0.1 < z < 0.8. The gray shaded region indicates separationsr < 40 Mpc, where the analytical modebreaks due to the nonlinear regime.

#### E. Covariance matrix

We estimate the covariance matrix of the binned PKSZ measurement directly from the data using two resampling techniques:

(i) Jackknife: The jackknife resampling technique (labeled "JK" in equations) consists of measuring N<sub>JK</sub> subsamples removing one of them, and re-N<sub>JK</sub> – 1 subsamplesThis process is repeated until measurement. Then we estimate the covariance matrix as

$$\hat{C}_{ij}^{JK} \frac{1}{4} \frac{N_{JK} - 1}{N_{JK}} \frac{\cancel{N}_{JK}}{\alpha_{441}} \hat{\eth} \hat{T}_{i}^{\alpha} - \bar{T}_{i} \triangleright \hat{\eth}_{j}^{\alpha} - \bar{T}_{j} \triangleright; \quad \check{\eth} 11 \triangleright$$

where  $\hat{T}_i^{\alpha}$  is the pairwise KSZ signalin separation bin i and jackknife realization α, of metan For our main analysis,we use N<sub>JK</sub> ½ 1; 000 subsamples.

(ii) Bootstrap: The bootstrap method (indicated by "BS" in equations) consists of randomly drawing with replacementan equal number of clusters, and This process is repeated, times, and the covariance matrixĈ<sub>ii</sub>BS estimated as

 $\hat{C}_{ij}^{BS} \frac{1}{N_{BS}-1} \underbrace{\hat{\mathbf{N}}_{BS}}_{\text{GV1}} \hat{\mathbf{O}} \hat{\mathbf{T}}_{i}^{\alpha} - \bar{\mathbf{T}}_{i} \triangleright \hat{\mathbf{O}}_{j}^{\alpha} - \bar{\mathbf{T}}_{j} \triangleright :$ 

Here i and j refer to the separation bin,  $\hat{T}_i^{\alpha}$  is the estimated PKSZ signaln bin i for the α random sample, and Ti the average PKSZ value across all samples. The bootstrap method is expected to need more random samples than the jackknife method to converge due to random sampling. As a result, it is more computationally expensive. We use N<sub>BS</sub> 1/4 10;000 samples when reporting results with the bootstrap covariance.

The baseline covariance matrix in this work is estimated using the jackknife subsampling technique with 1,000 the PKSZ signal by splitting the cluster catalog into subsamplesand the correlation matrix derived from its shown in Fig. 4. As a test of robustnesswe also show computing the PKSZ amplitude from the remaining selected results when the covariance is estimated from a different number of subsamples or the bootstrap technique. every subsample has been discarded once from the We show in Fig. 5 a comparison of the PKSZ error bars calculated from the two methods. Both estimators have clearly converged and show minimal differences in the covariance valuesbetween N<sub>JK</sub> 1/4 1;000 or 2,000, and  $N_{BS}$  ¼ 4;000 or 10,000. The bootstrap estimatoryields larger uncertainties at small separation distances, however the differences are within allowable tolerances for the current signal-to-noise ratio.

For the inverse of the covariance use the estimator

$$\tilde{C}^{-1} \frac{1}{4} \frac{N - N_{bins} - 2}{N - 1} \hat{C}^{-1};$$
 ð13F

where N is the number of jackknife or bootstrap samples recomputing the PKSZ signal for each random drawused to compute the covariance macrix=BS, and Nins is the number of comoving separation bins. his correction factor is needed because the empirically determined inverse

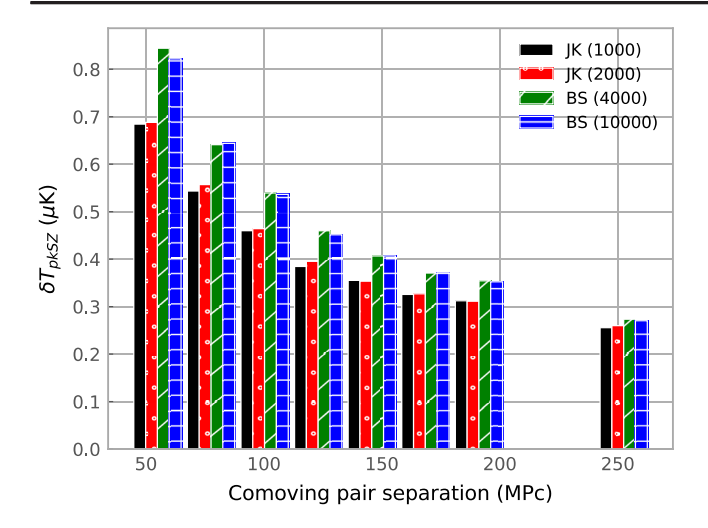


FIG. 5. Estimated uncertainties from JK and BS covariance estimators for 1000=2000 subsamples and 4000=10000 resamplings, respectively. The error estimate is stable across the different methods and number of subsamples/resamples/le construct this figure from the SPT-3G b DES-Y3 data.

covariance matrix $\hat{\mathbb{C}}^{-1}$  is a biased estimator of the true inverse covariance matrix  $\hat{\mathbb{C}}$  as shown in [51].

#### F. Model fitting and statistical significance

We fit the measured PKSZ signato a one parameter model, scaling the analytical template given by Eq. (10) by the unknown average optical depth of the cluster sample. We then compute the statistical significance of our measurement in two different ways:

(1) The main results will be presented by obtaining the best-fitre and its uncertainty by minimizing theak

$$\begin{split} \chi^2 \tilde{\delta r_e} & \triangleright 1/4 \, \hat{T}_{PKSZ} - T_{PKSZ} \tilde{\delta r_e} & \triangleright^\dagger \\ & \times \tilde{C}^{-1} \hat{\mathcal{R}}_{PKSZ} - T_{PKSZ} \tilde{\delta r_e} & \triangleright : \quad \eth 14 \\ \end{split}$$

The signal-to-noise ratio S=N is then computed with S=N  $\sqrt[4]{\tau_e} = \sigma_{\overline{t_e}}$ , where  $\sigma_{\overline{t_e}}$  is given by  $\chi^2 \delta \overline{\tau_e}$   $\sigma_{\overline{t_e}} \triangleright - \chi^2_{\min} \sqrt[4]{1}$ .

(2) To complement the previous significance we also assess the signalignificance by calculating the  $\frac{2}{\chi}$  with respect to the null-signal hypothesis:

We estimate the probability to exceed (PTE) the observed  $\chi_0^2$  by comparing it to the cumulative distribution function of the  $\chi^2$  distribution. The PTE provides one estimate for how likely it is that the data could resulfrom a noisy measurement zero PKSZ signal.

We expect the template fit to yield a higher statistical significance than the null-signal procedure due to the fact that the first one includes the additional information of our analytic template, whereas the latter one makes no assumptions about the expected signal shape.

#### V. SIMULATIONS

#### A. Simulations of the mm-wave sky

In order to validate and test the accuracy of our analysis pipeline, as well as to estimate the impact systematic effects, we use realistic realizations of the millimeter wavelength sky from the MDPL2 Synthetic Skies suite [52]. The simulated skies are generated by pasting astrophysical effects onto the halo light cone from the MultiDark Planck 2N-body simulation [53]. The astrophysical modfling in the simulation has been calibrated using observational data and external hydrodynamical simulations. Outlined below are the main components of the simulated microwave sky:

- (i) The dark matter density field is used to gravitationally lens the CMB sky.
- (ii) The TSZ signal from each dark matter halo is added based on the [54] electron thermal pressure profile that was calibrated on the hydrodynamical BAHAMAS simulations suite [55].
- (iii) The KSZ effect is added in a similar way. The same [54] gas profile is used to estimate the electron number densitywhich is multiplied by the line-of-sight velocity to obtain the KSZ signal from the halo.
- (iv) The CIB from dust-enshrouded galaxies is simulated by first assigning star formation rate and stellar mass to each individual halo using the UniverseMachine code [56]. With that information, the bolometric infrared luminosity is inferred from [57], and then converted to flux density assuming the shape of the spectral energy distribution to be a modified blackbody.
- (v) We add instrumental noise to the simulations, assuming white noise levels of 7, 5, and 20 μK-arcmin at 90, 150, and 220 GHz, respectively. These noise levels are similar to the real data maps at the angular scales of interes \$000 < I < 5000.

(see SecIII B).

#### B. Pipeline validation

We now use the simulation suite introduced above to presence of contaminating signals and the noise level in the  $\frac{1}{2}$   $\frac{1}{4}$  0.01. dataset.

We check how the instrumental noise level of the 150 GHz map affects the recovered PKSZ signas well as the impact of photometric redshift uncertainties the measured KSZ amplitude and report our findings in Table

We extract the temperature at the clusters' positions for this test using the single frequency matched filter and use the same range of scales as the one adopted for the real analysis

described in Sec. IVA. As expected, we find that decreas-TABLE III. Effect on the PKSZ S=N of the CIB subtraction by ing the instrumental noise levels translates to an increase increasing its powerin the covariance matrix for the matched detection significance; however, when we include the redshift errors ( $\sigma_7 > 0$ ) the significance level does not improve. This indicates that redshift uncertainties pose an jection, and -CIB stands for a CIB reduction following [60] for intrinsic limit to this analysis. We also choose a noise level sampled are described in the last paragraph of Sec. of 18 µK-arcmin to approximate the noise leveror the SPT-SZ CMB maps used in the analysis of [23]. They estimated a signal from a different set of simulations [59] 3.7 $\sigma$ , with a mass range of 0.9 < M<sub>500c</sub>= $\delta$ 10<sup>4</sup>M<sub> $\odot$ </sub> $\triangleright$  < 4. We obtain within the same mass range a S=N of 3.8σ, agreeing with their estimates and giving us confidence in the simulations that we are using. The 5 µK-arcmin corresponds approximately to the currentoise levels of the 150 GHz map with one year of the SPT-3G data. From with a noise penalty that may be larger than the TSZ now on, we will use of 0.01 since it is approximately the contamination itself particularly for lower-mass clusters.

on the statistical uncertainties by running the extraction pipeline on maps that have primary CMBTSZ, and CIB set to zero one by one, while keeping the rest of the foregrounds unchanged for the 150 GHz makemoving the foregrounds clearly helps to improve the signal as in an increase in the S=N ratio by 25%. To remove the of MF-MFs, including a version in which the particular frequency dependence of the TSZ is used to deproject explicitly (MF-TSZ). This deprojection, however, comes

TABLE I. Impact of the 150 GHz map instrumental noise levels on the S=N of PKSZ. We see how lowering the map noise level increases the detection significance of the signal, but the photometric redshifterror σ<sub>z</sub> dominates the signalThese results are obtained by including all the cosmological and foreground components (CMB,TSZ, CIB) with the noise levels noted on the first column.

Noise level (µK-arcmin)	S=N (o <sub>z</sub> 1/4 0)	S=N (o <sub>z</sub> 1/4 0.01)
18	7.8	3.8
5	10.4	3.9

TABLE II. Effect of different foreground removalson the 150 GHz map on the S=N of PKSZ, where all the results are explore the sensitivity of the pairwise KSZ estimator to the poise levels to 5 μK-arcmin and include photo-z errors with

	Foreground removed	S=N	
	TSZ	4.8	
	CMB	5.3	
I.	CIB	4.3	

filter construction.MF-MF stands for matched filter multifrequency, MF-TSZ stands for matched filter with a TSZ depro-

Method	Simple sample	Mixed sample
₹ F-MF	3.6	3.4
MF-TSZ	4.0	3.8
MF-TSZ-CIB	3.6	3.8
MF-MF-CIB	3.2	3.2

root mean square photo-z error for the DES cluster catalog Finally, we also artificially increase the CIB signal power by a factor of 5 in the noise covariance used for the We also investigate the impact of different foregrounds multifrequency matched filter with and without TSZ deprojection (MF-TSZ-CIB and MF-MF-CIB, respectively) in an attempt to reduce its effect as shown in [60]. We tested a mix (mixed sample) of the cluster signal where the low-mass clusters (0.6 <  $M_{0.00}$ =10<sup>14</sup> $M_{\odot}$  < 1) are extracted from the single frequency matched filtered shown in Table II. In particular, the removal of TSZ results 50 GHz map (N 1/4 14, 321), while the high mass clusters'  $(1 < M_{500c} = 10^{14} M_{\odot} < 4)$  temperatures are extracted from contamination from cluster TSZ signal, we explore the use the TSZ deprojected multifrequency matched filtered map (N ¼ 8; 602). We obtain similar significance levels with all the different matched filters and cluster samples, with results shown in Table III. Since the significance levels are similar, we will not try to suppress the CIB in the SPT-3G data.

#### VI. PAIRWISE KSZ MEASUREMENT

#### A. Pairwise KSZ signal from SPT and DES

The pairwise KSZ measurement from SPT-3G maps and the full DES Year-3 redMaPPer cluster catalog in the 10 <  $\tilde{\lambda}$  < 60 richness range (N ½ 24, 580) is presented in Fig. 6. This result has been obtained by combining the temperatures extracted from the TSZ deprojected map for high richness clusters (30 \* < 60) and temperatures extracted

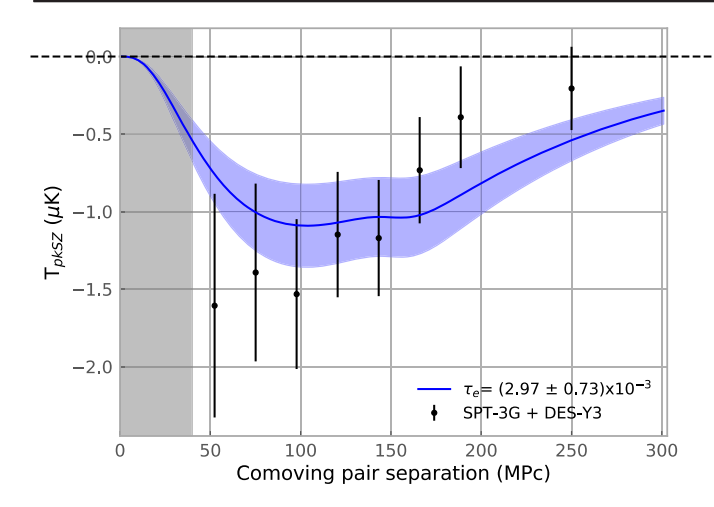


FIG. 6. We detect the PKSZ signal at 4.1σ, using the covariar estimated with the jackknife method and 1,000 subsampless. described in SecIV E, the 150 GHz SPT-3G map is used for low-richness clusters ( $\lambda \leq 30$ ) while a multifrequency matched filter TSZ-free map is used for high-richness clusters ( $\lambda > 30$ ). The recovered mean optical depth of the cluster sample is  $\bar{\tau}_e$  ¼ ð2.97 0.73Þ × 10³. The gray shaded region indicates the scales (r < 40) Mpc where the analytical model breaks due to the nonlinear regime.

from the matched filtered 150 GHz map for lower richness clusters  $\tilde{h}$  < 30). As discussed in SeclV F, we estimate and report a detection at a significance of 4.1 $\sigma$ . The resultiethness range 20  $<\tilde{\lambda}$  < 60. The results of this test are the fit to the analytical pairwise KSZ template yields a cluster catalog mean optical depth of

$$\bar{T}_{e}$$
 ¼ ð2.97 0.73Þ × 10<sup>3</sup>: ð16Þ

The corresponding correlation matrix between different radial separations shown in Fig. 4. [23] found T<sub>e</sub> 1/4  $\delta$ 1.37 0.41 ▷ × 10<sup>-3</sup> for the same richness range and 28,760 clusters using SPT-SZ and the DES-Y1 cluster catalog, which is  $\sim 2\sigma$  lower than the value we find. Another previous analysis [24] found \$\frac{1}{4}\$ \dot{0}.69 0.34 \to \times\$  $10^{-4}$  for a mass range of  $1 < M_{200c} = 10^{13} M_{\odot} < 1.6$ . The average mass of these clusters is an order of magnitude less massive than the estimated mass of our catalog  $0.6 \le M_{500c}$ = $10^{14} M_{\odot} < 4$ , thus finding a higher value of the  $\overline{\tau_e}$  in our analysis is consistent.

As noted earlier, the total significance of the PKSZ detection in this work  $(4.1\sigma)$  is similar to that from [23] (4.2σ), despite a large improvement in CMB map noise. As(iji) discussed in SecV B, this is because the redshift incertainties pose an intrinsic limit to the analysis.

As a consistency check, we compare the detection significances obtained using the alternative matched filters to the SPT-3G maps to extract the temperature at the clusters' positions and then we reconstructhe pairwise

TABLE IV. The mean opticable  $T_e \times 10^3$  and the S=N of each one in parenthesis, for two main richness cuts taken on the DES catalog for this analysis. The different methods to extract the temperature at the clusters' positions are explained in Sec. V B. "MF-150 GHz" stands for a matched filter for only the 150 GHz temperature map, "MF-MF" stands for matched filter multifrequency, "MF-TSZ" stands for matched filter with a TSZ deprojection,and "Mixed" stands for the mixed catalog of low mass clusters coming from the MF-150 GHz and higher mass clusters coming from the MF-TSZ. The baseline result of the paper is highlighted in bold.

	10 < λ̃ < 60	20 < λ̃ < 60
Method	(N 1/4 24; 580)	(N ¼ 5; 797)
MF-150 GHz	3.08 0.75 (4.1)	2.39 1.65 (1.4)
MF-MF	2.85 0.89 (3.2)	2.16 2.13 (1.0)
nMeF-TSZ	3.72 1.15 (3.2)	2.61 2.03 (1.3)
Mixed	2.97 0.73 ð4.1Þ	2.66 1.65 (1.6)

KSZ for each of them. The results of the fits to the analytical PKSZ template are displayed in Table IVAs can be seen, all the  $\bar{\tau}_e$  values are well within the  $1\sigma$ statistical uncertainties of each other and the corresponding detections shift by less than  $0.5\sigma$ .

Finally, we explore how the detection is affected by a higher low-mass threshold by repeating the analysis for the reported in the right column of Table IV, where we can clearly see that the significance of the detection has decreased greatly due to the limited number clusters that fall in this richness range, thus increasing the estimated errors on the measurements.

#### B. Null tests

We run a suite of null tests that check whether the signal present in the data has statistical properties consistent with the pairwise KSZ effect

- (i) Sign flip: For this test, we replace the minus sign inside the sum in the estimator in Eq. (4) with a plus sign to remove sensitivity to the PKSZ signal.
- (ii) Position shuffling: By randomly shuffling the redshifts of the clusters while keeping their extracted temperatures unchanged, we null the pairwise signal by making c<sub>ii</sub> maximum on clusters that are not under the gravitational influence of each other.
- Temperatureshuffling: We randomly shuffle the clusters' extracted temperature without changing their position, keeping the same for the estimator and thus removing the pairwise signal from the clusters.

introduced in Sec. IV B. We first apply these matched filters As shown in Fig. 7, the null tests remove the pairwise KSZ signal, leaving a mean-zero signal ith correlated uncertainties as encoded in the covariance matrix. To quantify the

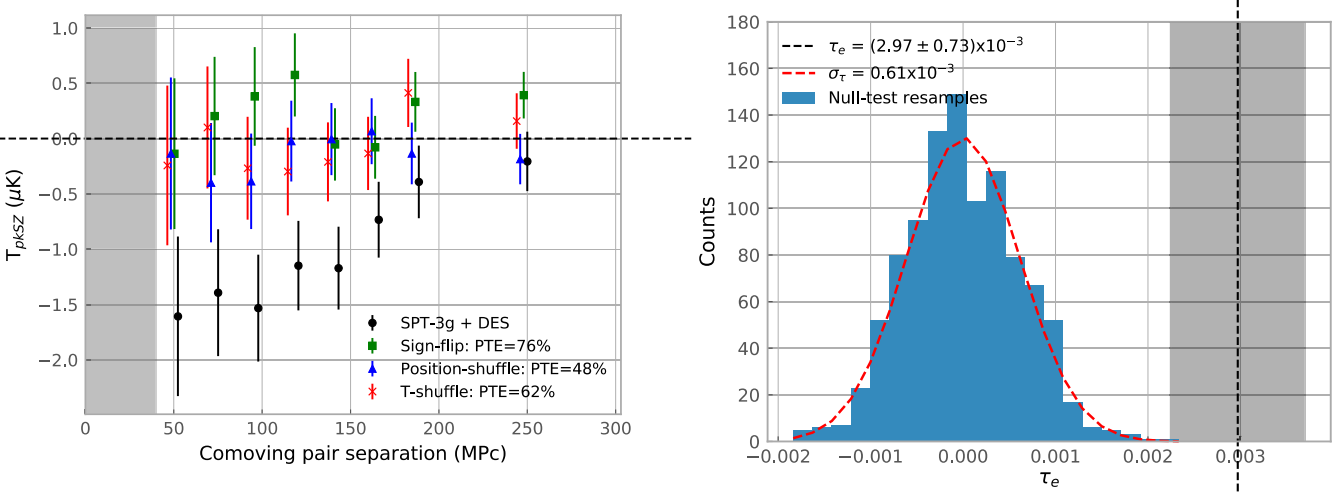


FIG. 7. Null tests for the SPT – 3G b Full DES catalog PKSZ measurements. All the null-tests yield a reduced 1x and their data points measured of the PKSZ signal for our baseline analysis. The points are offset in comoving separation for visualization purposes.

result of these tests we calculate the reduced for each bootstrap resample in each test, and we quote the PTE as the fraction of bootstrap resamples with reduced > 1. We obtain PTEs of 76%, 48%, and 62% for the sign flip, distance shuffling and temperature shuffling, respectively, with a mean reduced $^2\chi$ ~ 1 for each of the tests. These null tests are consistent with no detection, giving us confidence in our

We also use the null test bootstrap resamples as a check of our formal estimate of the uncertainty on We display the distribution of bootstrap resamples forthe sign-flip test in Fig. 8; the distributions for the other tests look similar. The estimated error of the mean optical depth from real data is comparable with our null tests errors within ~20%, which gives us confidence on the accuracy of the measurement.

measurement of the pairwise KSZ effect.

## C. Systematics tests

We test some systematicsthat could influence our measurement f the PKSZ signal in order to quantify any impact on our analysis and subsequent measurements.

(i) Mass scatter: In order to match the mass range from simulations, where the masses of clusters are known, to the optical cluster catalog that is selected in richness,we need a good understanding of how to obtain an accurate representation of the mass ranges under analysis. This is of particular interest because the analytical model in Eq. (3), which is used to infer the clusters' optical depth, depends on the mass range of interest and changing the typical cluster mass could significantly bias this result. In this work we have selected the simulation sample using the relation shown in [58]. However, we need to take

FIG. 8. Histogram of 1,000 bootstrap resamples for the sign-PTE values are reported in the legend. The black points are the lip test estimating, comparing them to the baseline result of shown in the dashed black line, with the gray region representing the  $1\sigma$  uncertainty. This histogram shows us how a resampling of null tests produces an estimated Gaussian error the  $\bar{\tau}_e$  of  $\sigma_{\overline{t}_a}$  ¼ 0.61 × 10<sup>3</sup>, which is a ~20% difference to the one obtained for the readata of  $\sigma_{12}$  ¼ 0.73 × 10<sup>3</sup>.

into account that these are estimated measurements, therefore a scatter in the cluster mass of the optical data can occur. To model this scatter, we draw mass errors from a normal distribution with width σ<sub>InδMP</sub> 1/4 0.3, which is an underestimation of the scatter atlow richness for a Gaussian error model given the significant projection effects in the DES sample [45,61–63], but it gives an idea of how significant the mass scattering can be. We then use these errors to compute the PKSZ signation the simulations, obtaining an average decrease on the signal detection to 2.5σ on the simulation catalog for the mass range of 0.6 <  $M_{500c}$ =10<sup>14</sup> $M_{\odot}$  < 4. This implies that the measured PKSZ significance might be  $\sim 1\sigma$  lower than it could be due to this effect.

(ii) Mis-centering: The measured PKSZ signatan be diluted due to the fact that the clusters' positions estimated from the optical survey catalog might not coincide with the location of the cluster KSZ signal. This mis-centering has a larger impactin clusters that are not fully relaxed or are merging, where the potential minimum is not located on the brightest cluster galaxy, or where this galaxy has been misidentified by the redMaPPeralgorithm. The impact of mis-centering has been tested before [23], where two different mis-centering models [46,64] were tested and identified a reduction of ~10% of the PKSZ significance Although for our confidence levels itdoes not produce a significant impact, it should be considered for future spectroscopic redshift catalogs.

# D. Estimating the optical depth from the thermal SZ effect

In addition to the bulk velocity of electrons, the electrons' random thermal motion imprints a signature on the observed CMB through inverse-Compton scattering,

For the signal-to-noise-maximizing filter scale of 402.6, effect produced along a line-of-sight; can be quantified by the Compton y parameter [66],

$$Z$$
  $y \tilde{\alpha} \hat{n}_i P \frac{k_B T_e}{m_e c^2} \sigma_T;$   $\tilde{\sigma} 17 P$ 

where kg is the Boltzmann constant, this the mass of the electron, and  $\pi$  is the electron temperature. The TSZ effectompute the aperture photometry with  $\theta$  ½ 2.6 to the induces a frequency-dependent shift of the observed CMBecovered filtered y map and the original one. We then temperature, which in the nonrelativistic limit can be written as

with gov  $\frac{1}{4}$   $\frac{1}{8}$   $\frac{1}{8}$  - 4 and x  $\frac{1}{4}$  hv= $\frac{1}{8}$  hv= $\frac{1}{8}$  hv. The frequency dependence of the TSZ effect is such that the effect appears as a temperature decrement at lower frequently lues of the clusters, while the systematic errors are cies than ~218 GHz, while being completely null at that frequency value [4]. Since the TSZ is directly related to the alues (syst) Inοτορ and m, which are 2% and 6%, electron pressure (number density of lectrons times the electron temperature of the cluster, the signal becomes stronger for more massive clusters.

We build a v map by performing an internal linear combination [67] on the 90, 150, and 220 GHz temperatures the Compton-y estimate of the mean optical pth to maps from SPT-3G. This y map is preliminary and has no preak the degeneracybetween the optical depth and been fully optimized, but we are primarily concerned with velocity in the PKSZ signal, and significantly improve the mean value of cluster optical depth, and a nonoptimizests of cosmology from the PKSZ effect. y map will mainly result in elevated variance, and not bias, in the optical depth measurement bring this y map, we stack all our clusters and extract the average y value through aperture photometry. The aperture photometry filter is written in real space as

inside the disc of radius  $\theta$ n contrast to the matched filter sample (10 <  $\tilde{\lambda}$  < 30), and a constrained matched filter technique described in Sec. IV B, this approach does not to zero the nonrelativistic TSZ effect for more massive assume a specific model for the cluster profile; however itclusters (30  $<\tilde{\lambda}$  < 60). requires that the cluster is contained within the characteristic filter scale & to avoid biases in the temperature

estimation.

where  $\theta_r$  is the characteristic filter scale. The aperture

We follow [28] and relate the mean y value of the clusters to the mean optical depthe according to

Ref. [28] calibrated the coefficients to be Inop ¼ −6.47 and m  $\frac{1}{4}$  0.49.

The transfer function and beam applied to the SPT-3G temperature maps described in Selc.produce a bias for object-based analysis such as aperture photometry [60]. To estimate this bias we applied the same transfer function and beam filters to the set of simulations in Sec. VA. We compute there finding a 10% reduction of the measured filtered value in comparison with the original simulation y map. Taking this into account we find

where we estimate the statistic (stat) uncertainty of this measuremently performing 1,000 JK resamples to the y obtained by propagating the uncertainty from the calibrated respectively.

The Compton-y-based estimate the mean optical depth is within 0.6σ of the PKSZ-derived estimate of  $\bar{\tau}_e$  ¼ ð2.97 0.73Þ × 10<sup>3</sup>. Future works will be able to

# VII. CONCLUSIONS

In this work, we measure the mean optical depth of the DES-Y3 redMaPPercluster sample in the 10 <  $\lambda$  < 60 richness range and between 0.1 < z < 0.8 and find the depth measurement is derived from a 4.1 $\sigma$  detection of the pairwise KSZ effect. The SPT-3G and DES surveys overlap over ~1; 400 deg of southern sky, and after cuts, there are 24,580 galaxy clusters from the DES-Y3 redMaPPer cluster sample within the SPT-3G survey region. We extract photometry effectively reduces the noise on all scales thathe CMB temperature shift at the location of these clusters are larger than the filter scale by subtracting the average using a matched filter approach to optimize signal-to-noise temperature in the outer ring from the average temperature the 150 GHz maps for the low-mass end of the cluster

> We validate the analysis using simulated data from the MDPL2 simulation suite [52]. We also use these simulations to explore the limiting uncertainties in the analysis,

finding the major sources of uncertainty in the current dataset to be due to uncertain cluster redshifts aifthot removed the TSZ effect in massive clusters. This result motivates the decision to use a constrained matched filterthe U.S. Departmentof Energy ContractNo. DE-AC02zero the thermal SZ signal in clusters with a richness  $\tilde{\lambda} > 30$ . There are also non-negligible contributions from and instrumental noise.

analysis using different methods of temperature extraction funding for the DES Projects has been provided by the finding agreement between the recovered optical depth and S. Departmentof Energy, the U.S. National Science the S=N levels. We also found an agreement on optical deputation, the Ministry of Science and Education of when increasing the minimum richness (20 <  $\tilde{\lambda}$  < 60), although with a lower significance on the PKSZ signal due to fewer clusters in this cut. To provide further evidenter England, the National Center for Supercomputing of the robustness of our results, we have conducted differ Applications at the University of Illinois at Urbananull tests where we artificially remove any cosmological signal and found the recovered PKSZ measuremente consistent with zero.

of the cluster sample from the PKSZ measurement to oneat Texas A&M University. Financiadorade Estudos e obtained based on the mean Compton y parameter as described in [28], finding the two estimates agree within 0.6σ. This demonstrates the application of using the observed thermal SZ signal to break the degeneracy between the mean optical depth and velocity for the PKSZ effect. The combination of upcoming CMB and spectroscopic surveys is expected to yield high significan pestitutions are Argonne National Laboratory, the measurements of the PKSZ signal.

By breaking the degeneracy with astrophysics using alternative techniques like this, we can proceed to constrained to constrained in the University cosmological parameters using the PKSZ; however, for this Chicago, University College London, the DES-Brazil to occur a higher signal-to-noise ratio of the PKSZ signal isonsortium, the University of Edinburgh, the required. Assuming current SPT-3G CMB map noise levels, we expect that future spectroscopic catalogs will significantly reduce clusters' redshift incertainty, leading to an increase of the PKSZ signal to  $\sim 10\sigma$ . This will increase further in future CMB experiments with higher skgnergies, Lawrence Berkeley National Laboratory, the coverage and lower noise levels.

#### **ACKNOWLEDGMENTS**

SPT is supported by the NationalScience Foundation through Grants No. PLR-1248097 and No. OPP-1852617of Pennsylvania, the University of Portsmouth, SLAC Partial support is also provided by the NSF Physics Frontileational Accelerator LaboratoryStanford University,the Center GrantNo. PHY-1125897 to the KavliInstitute of Cosmological Physics at the University of Chicago, the Kavli Foundation and the Gordon and Betty Moore Foundation Grant No. GBMF 947. This research used resourcesof the National Energy ResearchScientific Computing Center(NERSC), a DOE Office of Science User Facility supported by the Office of Science of the U Department of Energy under Contract No. DE-AC02-05CH11231. The Melbourne group acknowledges supporported by the National Science Foundation under from the Australian Research Council's Discovery Project@rants No. AST-1138766 and No. AST-1536171. The scheme (Grant NoDP200101068)B. B. is supported by

the Fermi Research Alliance LLC under Contract No. De-AC02- 07CH11359 with the U.S.Department of Energy. Argonne National Laboratory's work was supported under 06CH11357. We also acknowledge support from the Argonne Centerfor Nanoscale Materials. This research the primary CMB anisotropy, cosmic infrared background was done using services provided by the OSG Consortium [68,69], which is supported by the National Science We test the robustness of the detection by repeating the Foundation Grants No. 2030508 and No. 1836650. Spain, the Science and Technology Facilities Council of the United Kingdom, the Higher Education Funding Council Champaign, the Kavli Institute of Cosmological Physics at the University of Chicago, the Center for Cosmology and Astro-Particle Physics atthe Ohio State University, the Finally, we compare our result for the mean optical depthitchell Institute for Fundamental Physics and Astronomy Projetos, Fundação Carlos Chagas Filho de Amparo `a Pesquisa do Estado do Rio de Janeiro, Conselho Nacional de Desenvolvimento Científico e Tecnológico and the Ministério da Ciência, Tecnologia e Inovação, the Deutsche Forschungsgemeinschaftd the Collaborating Institutions in the Dark Energy Survey. The Collaborating University of California at Santa Cruz, the University of Cambridge, Centro de Investigaciones Energéticas, EidgenössischeTechnischeHochschule (ETH) Zürich, Fermi National Accelerator Laboratorythe University of Illinois at Urbana-Champaigrthe Institut de Ciències de l'Espai (IEEC/CSIC), the Institut de Física d'Altes Ludwig-Maximilians UniversitätMünchen and the associated Excellence Cluster Universe, the University of Michigan, NFS's NOIRLab, the University of Nottingham, The Ohio State University, the University University of Sussex, Texas A&M University, and the OzDES Membership Consortium. Based in part on observations at Cerro Tololo Inter-American Observatory at NSF's NOIRLab (NOIRLab Prop. ID 2012B-0001; PI: J. Frieman), which is managed by the Association of Universities for Research in Astronomy (AURA) under a Sooperative agreement with the National Science Foundation. The DES data management ystem is sup-DES participants from Spanish institutions are partially

No. PGC2018-094773No. PGC2018-102021No. SEV-2016-0588, No. SEV-2016-0597 and No. MDM-2015-0509, some of which include ERDF funds from the European Union. I. F. A. E. is partially funded by the CERCA program of the Generalitat de Catalunya. Research leading to these results has received funding from from the artnership for Advanced Supercomputing in Europe Seventh Framework Program (FP7/2007-201ia)cluding ERC Grant AgreementsNo. 240672, No. 291329, and No. 306478. We acknowledge suppoftom the Brazilian Instituto Nacionalde Ciência e Tecnologia (INCT) do e-Universo (CNPg GrantNo. 465376/2014-2). This manuunder ContractNo. DE-AC02-07CH11359 with the U.S. Departmentof Energy, Office of Science, Office of High

supported by MICINN under Grants No. ESP2017-89838, Energy Physics. The CosmoSim database used in this paper is a service by the Leibniz-Institute for Astrophysics Potsdam (AIP). The MultiDark database was developed in cooperation with the Spanish MultiDark Consolider Project No. CSD2009-00064. The authors gratefully acknowledge the Gauss Centre for Supercomputing e.V[70] and the the European Research Council under the European Unid PRACE [71]) for funding the MultiDark simulation project by providing computing time on the GCS Supercomputer SuperMUC at Leibniz Supercomputing Centre (LRZ [72]). The Bolshoi simulations have been performed within the Bolshoi project of the University of California High-Performance AstroComputing Cente(UC-HiPACC) and script has been authored by Fermi Research Alliance, LLWere run at the NASA Ames Research Center. We acknowledge the use of many PYTHON packagesiPYTHON [73], MATPLOTLIB [74], and SCIPY [75].

- [1] R. A. Sunyaev and Y. B. Zel'dovich, Astrophys. Space Sci[16] W. J. Percival and M. White, Mon. Not. R. Astron. Soc. 393, 7, 3 (1970). 297 (2009).
- [2] R. Sunyaev and Y.Zel'dovich, Annu. Rev. Astron. Astrophys. 18, 537 (1980).
- [3] M. Birkinshaw, Phys. Rep. 310, 97 (1999).
- [4] J. E.Carlstrom, G. P.Holder, and E. D.Reese Annu. Rev. Astron. Astrophys. 40, 643 (2002).
- [5] S. Das, T. Louis, M. R. Nolta, G. E. Addison, E. S. Battistelli, J. R. Bond, E. Calabrese, D. Crichton, M. J. Devlin, S. Dicker et al., J. Cosmol. Astropart. Phys. 04 (2014) 014.
- [6] C. L. Reichardt, S. Patil, P. A. R. Ade, A. J. Anderson, J. E. Austermann, J. S. Avva, E. Baxter, J. A. Beall, A. N. Bender, B. A. Benson et al., Astrophys. J. 908, 199 (2021)[20] S. Padin, Z. Staniszewski, R. Keisler, M. Joy, A. A. Stark,
- [7] T. M. Crawford, K. K. Schaffer, S. Bhattacharya, K. A. Aird, B. A. Benson, L. E. Bleem, J. E. Carlstrom, C. L. Chang, H.-M. Carlstrom et al., Appl. Opt. 47, 4418 (2008). Cho, A. T. Crites et al., Astrophys. J. 784, 143 (2014).
- [8] W. R. Coulton, S. Aiola, N. Battaglia, E. Calabrese S. K. Choi, M. J. Devlin, P. A. Gallardo, J. C. Hill, A. D. Hincks, J. Hubmayr et al., J. Cosmol. Astropart. Phys. 09 (2018)
- [9] N. Huang, L. E. Bleem, B. Stalder, P. A. R. Ade, S. W. Allen, A. J. Anderson, J. E. Austermann, J. S. Avva, J. A. Beall, A. N. Bender etal., Astron. J. 159, 110 (2020).
- [10] M. Hilton, C. Sifón, S. Naess, M. Madhavacheril, M. Oguri, E. Rozo, E. Rykoff, T. M. C. Abbott, S. Adhikari, M. Aguena etal., Astrophys.J. Suppl. Ser. 253, 3 (2021).
- [11] L. D. Shaw, D. H. Rudd, and D. Nagai, Astrophys. J. 756, 15 (2012).
- [12] O. Lahav, M. J. Rees, P. B. Lilje, and J. R. Primack, Mon. Not. R. Astron. Soc. 251, 128 (1991).
- [13] M. G. Haehnelt and M. Tegmark, Mon. Not. R. Astron. Soq26] J. C. Hill, S. Ferraro, N. Battaglia, J. Liu, and D. N. Spergel, 279, 545+ (1996).
- [14] Y.-Z. Ma and G.-B. Zhao, Phys. Lett. B 735, 402 (2014).
- [15] F. Bianchini and A. Silvestri, Phys. Rev. D 93, 064026 (2016).

- [17] D. S. Swetz, P. A. R.Ade, M. Amiri, J. W. Appel, E. S. Battistelli, B. Burger, J. Chervenak, M. J. Devlin, S. R. Dicker, W. B. Doriese et al., Astrophys. J. Suppl. Ser. 194, 41 (2011).
- [18] K. S. Dawson, D. J. Schlegel, C. P. Ahn, S. F. Anderson, É. Aubourg, S. Bailey, R. H. Barkhouser, J. E. Bautista, A. Beifiori, A. A. Berlind et al., Astron. J. 145, 10 (2013).
- [19] N. Hand, G. E. Addison, E. Aubourg, N. Battaglia, E. S. Battistelli, D. Bizyaev, J. R. Bond, H. Brewington, J. Brinkmann, B. R. Brown et al., Phys. Rev. Lett. 109, 041101 (2012).
- P. A. R.Ade, K. A. Aird, B. A. Benson, L. E. Bleem, J. E.
- [21] J. E. Carlstrom, P. A. R. Ade, K. A. Aird, B. A. Benson, L. E. Bleem, S. Busetti, C. L. Chang, E. Chauvin, H.-M. Cho, T. M. Crawford et al., Publ. Astron. Soc. Pac. 123, 568 (2011).
- [22] B. Flaugher, H. T. Diehl, K. Honscheid, T. M. C. Abbott, O. Alvarez, R. Angstadt, J. T. Annis, M. Antonik, O. Ballester, L. Beaufore et al., Astron. J. 150, 150 (2015).
- [23] B. Soergel, S. Flender, K. T. Story, L. Bleem, T. Giannantonio, G. Efstathiou, E. Rykoff, B. A. Benson, T. Crawford, S. Dodelson etal., Mon. Not. R. Astron. Soc. 461, 3172 (2016).
- [24] V. Calafut, P. Gallardo, E. Vavagiakis, S. Amodeo, S. Aiola, J. Austermann, N. Battaglia, E. Battistelli, J. Beall, R. Bean et al., Phys.Rev.D 104, 043502 (2021).
- [25] Z. Chen, P. Zhang, X. Yang, and Y. Zheng, Mon. Not. R. Astron. Soc. 510, 5916 (2022).
- Phys.Rev.Lett. 117, 051301 (2016).
- [27] E. Schaan, S. Ferraro, S. Amodeo, N. Battaglia, S. Aiola, J. E. Austermann J. A. Beall, R. Bean, D. T. Becker, R. J. Bond et al., Phys.Rev. D 103, 063513 (2021).

- [28] N. Battaglia, J. Cosmol. Astropart. Phys. 08 (2016) 058.
- [29] F. D. Bernardis, S. Aiola, E. Vavagiakis, N. Battaglia, M. Niemack, J. Beall, D. Becker, J. Bond, E. Calabrese, H. C/62 Y. Omori, arXiv:2212.07420. et al., J. Cosmol. Astropart. Phys. 03 (2017) 008.
- [30] E. Vavagiakis et al. Phys. Rev. D 104, 043503 (2021).
- [31] Planck Collaboration, N. Aghanim, Y. Akrami, M. Ashdown, J. Aumont, C. Baccigalupi, M. Ballardini, A. J. Banday, R. B. Barreiro, N. Bartolo, S. Basak et al., Astron [55] I. G. McCarthy, J. Schaye, S. Bird, and A. M. C.Le Brun, Astrophys.641, A6 (2020).
- [32] F. Bernardeau, S. Colombi, E. Gaztañaga, and R. ScoccimarroPhys.Rep. 367, 1 (2002).
- [33] A. Diaferio, R. A. Sunyaevand A. Nusser, Astrophys. J. Lett. 533, L71 (2000).
- Dolag, Mon. Not. R. Astron. Soc. 478, 5320 (2018).
- [35] R. Juszkiewicz, V. Springel, and R. Durrer, Astrophys. J. Lett. 518, L25 (1999).
- [36] R. K. Sheth, A. Diaferio, L. Hui, and R. Scoccimarro, Mon. Not. R. Astron. Soc. 326, 463 (2001).
- [37] S. Bhattacharya and A. Kosowsky, Phys. Rev. D 77, 083004 (2008).
- [38] R. Keisler and F. Schmidt, Astrophys. J. Lett. 765, L32 (2013).
- [39] E.-M. Mueller, F. de Bernardis, R. Bean, and M. D. Niemack, Astrophys. J. 808, 47 (2015).
- [40] J. A. Sobrin, P. A. R. Ade, Z. Ahmed, A. J. Anderson, J. S[62] J. Myles, D. Gruen, A. B. Mantz, S. W. Allen, R. G. Morris, Avva, R. Basu Thakur, A. N. Bender, B. A. Benson, J. E. Carlstrom, F. W. Carter et al., Proc. SPIE Int. Soc. Opt. Eng. 10708, 107081H (2018).
- [41] D. Dutcher, L. Balkenhol, P. A. R. Ade, Z. Ahmed, E. Anderes, A. J. Anderson, M. Archipley, J. S. Avva, K. Aylor, P. S. Barry et al., Phys. Rev. D 104, 022003 (2021).
- [42] M. R. Calabretta and E. W. Greisen, Astron. Astrophys. 395, 1077 (2002).
- [43] K. K. Schaffer, T. M. Crawford, K. A. Aird, B. A. Benson, L. E. Bleem, J. E. Carlstrom, C. L. Chang, H. M. Cho, A. T. Crites, T. de Haan etal., Astrophys.J. 743, 90 (2011).
- [44] E. S. Rykoff, E. Rozo, M. T. Busha, C. E. Cunha, A. Finoguenov, A. Evrard, J. Hao, B. P. Koester, A. Leauthaud, B. Nord, M. Pierre, R. Reddick, T. Sadibekova, E. S.Sheldon, and R. H. Wechsler, Astrophys. J. 785, 104 (2014).
- [45] E. S. Rykoff, B. P. Koester, E. Rozo, J. Annis, A. E. Evrard, S. M. Hansen, J. Hao, D. E. Johnston, T. A. McKay, and R. H. Wechsler, Astrophys. J. 746, 178 (2012).
- [46] A. Saro, S. Bocquet, E. Rozo, B. A. Benson, J. Mohr, E. S. Rykoff, M. Soares-SantosL. Bleem, S. Dodelson, P. Melchior et al., Mon. Not. R. Astron. Soc. 454, 2305 (2015).
- [47] E. Rozo, E. S. Rykoff, A. Abate, C. Bonnett, M. Crocce, C.[70] www.gauss-centre.eu. Davis, B. Hoyle, B. Leistedt, H. V. Peiris, R. H. Wechsler et al., Mon. Not. R. Astron. Soc. 461, 1431 (2016).
- [48] P. G.Ferreira, R. Juszkiewicz, H. A. Feldman, M. Davis, and A. H. Jaffe, Astrophys. J. 515, L1 (1999).
- [49] A. Cavaliere and R. Fusco-Femiano, Astron. Astrophys. 4974] J. D. Hunter, Comput. Sci. Eng. 9, 90 (2007). 137 (1976).
- [50] J. Erler, M. E. Ramos-Ceja, K. Basu, and F. Bertoldi, Mon. Not. R. Astron. Soc. 484, 1988 (2019).

- [51] J. Hartlap, P. Simon, and P. Schneider Astron. Astrophys. 464, 399 (2007).
- [53] A. Klypin, G. Yepes, S. Gottlöber, F. Prada, and S. Heß, Mon. Not. R. Astron. Soc. 457, 4340 (2016).
- [54] A. J. Mead, T. Tröster, C. Heymans, L. Van Waerbeke, and I. G. McCarthy, Astron. Astrophys. 641, A130 (2020).
- Mon. Not. R. Astron. Soc. 465, 2936 (2016).
- [56] P. Behroozi, R. H. Wechsler, A. P. Hearin, and C. Conroy, Mon. Not. R. Astron. Soc. 488, 3143 (2019).
- [57] R. C. Kennicutt, Jr., Annu. Rev. Astron. Astrophys. 36, 189
- [34] B. Soergel, A. Saro, T. Giannantonio, G. Efstathiou, and K[58] T. McClintock, T. N. Varga, D. Gruen, E. Rozo, E. S. Rykoff, T. Shin, P. Melchior, J. DeRose, S. Seitz et al., Mon. Not. R. Astron. Soc. 482, 1352 (2019).
  - [59] S. Flender, L. Bleem, H. Finkel, S. Habib, K. Heitmann, and G. Holder, Astrophys. J. 823, 98 (2016).
  - [60] L. E. Bleem, T. M. Crawford, B. Ansarinejad, B. A. Benson, S. Bocquet, J. E. Carlstrom, C. L. Chang, R. Chown, A. T. Crites, T. de Haan et al., Astrophys. Suppl. Ser. 258, 36 (2022).
  - [61] S. Grandis, J. J. Mohr, M. Costanzi, A. Saro, S. Bocquet, M. Klein, M. Aguena, S. Allam, J. Annis, B. Ansarinejad et al., Mon. Not. R. Astron. Soc. 504, 1253 (2021).
    - E. Rykoff, M. Costanzi, C. To, J. DeRose, R. H. Wechsler, E. Rozo, T. Jeltema, E. R. Carrasco, A. Kremin, and R. Kron, Mon. Not. R. Astron. Soc. 505, 33 (2021).
  - [63] H.-Y. Wu, M. Costanzi, C.-H. To, A. N. Salcedo, D. H. Weinberg, J. Annis, S. Bocquet, M. Elidaiana da Silva Pereira, J. DeRose, J. Esteves et al. Mon. Not. R. Astron. Soc. 515, 4471 (2022).
  - [64] D. E. Johnston, E. S. Sheldon, R. H. Wechsler, E. Rozo, B. P. Koester, J. A. Frieman, T. A. McKay, A. E. Evrard, M. R. Becker, and J. Annis, arXiv:0709.1159.
  - [65] R. A. Sunyaev and Y. B. Zel'dovich, Comments Astrophys. Space Phys2, 66 (1970).
  - [66] R. A. Sunyaev and Y. B. Zel'dovich, Comments Astrophys. Space Phys4, 173 (1972).
  - [67] J. Delabrouille and J. FCardoso, arXiv:astro-ph/0702198.
  - [68] R. Pordes, D. Petravick, B. Kramer, D. Olson, M. Livny, A. Roy, P. Avery, K. Blackburn, T. Wenaus, F. Würthwein et al., J. Phys. Conf. Ser. 78, 012057 (2007).
  - [69] I. Sfiligoi, D. C. Bradley, B. Holzman, P. Mhashilkar, S. Padhi, and F. Wurthwein, in 2009 WRI World Congress on Computer Science and Information Engineering (IEEE, New York, 2009), Vol. 2, pp. 428-432.

  - [71] www.prace-ri.eu.
  - [72] www.lrz.de.
  - [73] F. Pérez and B. E. Granger, Comput. Sci. Eng. 9, 21 (2007).

  - [75] P. Virtanen, R. Gommers, T. E. Oliphant, M. Haberland, T. Reddy, D. Cournapeau, E. Burovski, P. Peterson, W. Weckesser, Bright et al., Nat. Methods 17,261 (2020).